Digest Journal of Nanomaterials and Biostructures Vol. 6, No 4, October-December 2011, p. 1991-2000

DIMENSIONALITY ANALYSIS OF SUPPORTED Ni NANOCLUSTERS THROUGH XRD AND MAGNETIC MEASUREMENTS

N. ALDEA[a], V. REDNIC[a*], S. PINTEA[a], P. MARGINEAN[a], L. REDNIC[a], V. POP[b], E. DOROLTI[b], S. MACAVEI[a], F. MATEI[c]

[a]*National Institute for Research and Development of Isotopic and Molecular Technologies, Donath 65-193, 400293 Cluj-Napoca, Romania;*

[b]*Babes-Bolyai University, Faculty of Physics, Kogalniceanu 1, 400084 Cluj-Napoca, Romania;*

[c]*University of Agricultural Sciences and Veterinary Medicine, Calea Manastur 3-5, Cluj-Napoca, Romania*

The supported nickel catalysts were analyzed by X-ray diffraction and magnetization measurements in order to determine their global structure. The Ni/Al_2O_3 treated at 623 K and Ni/Cr_2O_3 treated at 923 K catalysts have been investigated. The X-ray diffraction analysis of the (111), (200), (220), (311) and (222) line profiles of Ni provides information about the average particle size, microstrains parameter as well as the particle size and microstrain distribution functions of the supported nickel catalysts. This information is obtained by Warren-Averbach method based on Fourier treatment of the single X-ray line profiles analysis and double Voigt method. The global structure is obtained using fitting methods, based on the generalized Fermi and Voigt functions for the approximation of the experimental X-ray line profiles. The size-dependent magnetic properties of supported nickel catalysts nanoparticles were studied taking into account their superparamagnetic behaviour. Magnetization simulations versus applied magnetic field have been realized in the framework of the Langevin model in order to calculate theoretical particle size distribution by comparison of the resulted model with experimental data.

(Received December 8, 2011; accepted December 20, 2011)

Keywords: X-ray diffraction, global structure, supported metal catalysts, Fourier transform, Langevin model, superparamagnetism

1. Introduction

X-ray diffraction is a well known and widely used technique for the structural investigation of the materials but the nanodimensionality analysis is often not an easy task. When we have to deal with nanostructured materials, for which usually it is not possible to obtain satisfactory intensity measurements of two order (hkl) profiles, the classical method of Warren and Averbach [1] is not applicable.

In this paper we developed a rigorous analysis of the X-ray line profile (XRLP) of the supported nickel catalysts in terms of Fourier transform. In our approach the zero strains assumption is not required in both cases of single [2] X-ray profile Fourier analysis and double Voigt method [3]. In the case of XRLP, the convolution of the true data function by the instrumental function produced by a well-annealed sample is described by Fredholm integral equation of the first kind [4]. A rigorous way for solving this equation is the Stokes method based on the Fourier transform technique. Besides the X-ray diffraction, it is well known that the magnetic behaviour of the small sized ferromagnetic materials differs from that of the corresponding bulk materials. Within the superparamagnetic regime of the small magnetic

*Corresponding author: vrednic@itim-cj.ro

nanoparticles, magnetic measurements combined with theoretical modelling can give useful information related to particle size distribution [5, 6]. The aim of the present paper is to perform a comparative dimensionality analysis of the investigated systems using two techniques: the powder X-ray diffraction and the magnetization analysis within the framework of the Langevin theory applied to the superparamagnetic materials.

2. Theoretical background

2.1. XRD analysis

The theoretical considerations regarding the X-ray diffraction pattern analysis were widely discussed in author's previous papers [7]. Very few aspects are reviewed here below. Based on Warren and Averbach theory [1] the general form of the Fourier transform of the true sample for cubic lattices is given [4] by:

$$F^{(s)}(L) = e^{-\frac{|L|}{D_{eff}(hkl)}}, \quad F^{(\varepsilon)}(L) = e^{-\frac{2\pi^2 \left\langle \varepsilon_L^2 \right\rangle_{hkl} h_0^2 L^2}{a^2}} \tag{1}$$

where $F^{(s)}(L)$ is the Fourier transform contribution about crystalline size and stacking fault probability, $F^{(\varepsilon)}(L)$ the Fourier transform contribution about microstrain of the lattice, $D_{eff}(hkl)$ the effective crystallite size, $<\varepsilon^2>_{hkl}$ the microstrain of the lattice and $h_0^2 = h^2 + k^2 + l^2$. The Generalized Fermi Function (GFF) [8] and the Voigt distribution [9] are used in case of single XRLP analysis while double Voigt method [3] for two *(hkl)* order is applied.

2.2. Magnetization analysis

Within the superparamagnetic regime, the magnetisation m_i of the isolated isotropic particle of volume v_i with a magnetic induction B due to applied magnetic field, can be expressed by Langevin relation

$$\frac{m_i}{M_s} = \coth\frac{M_s B v_i}{k_B T} - \frac{k_B T}{M_s B v_i} \tag{2}$$

where k_B is the Boltzmann constant , T the absolute temperature and M_s the spontaneous magnetization of the domain. If we consider that M_s is not a function of the crystallite size, it is equal to the bulk spontaneous magnetization of investigated material. This equation can be generalized if we consider that the whole volume of the sample is V_o it is formed from n_i particles of v_i volumes. In this case, the overall magnetization M is given by:

$$\frac{M}{M_{sample}} = \frac{\left[\sum_{i=1}^{\infty}\left(\coth\frac{v_i M_s B}{k_B T} - \frac{k_B T}{v_i M_s B}\right) n_i v_i\right]}{V_0} \tag{3}$$

In the case of a supported metal catalyst, we introduce a volume fraction ε of metallic nickel in the sample and we consider a probability distribution function p of the volumes. Thus, the previous relation can be generalized

$$M(B,T) = \frac{\varepsilon M_{sample}\int_0^{\infty} V(D) L\left(\frac{M_s V(D) B}{k_B T}\right) p(D)\, dD}{\int_0^{\infty} V(D)\, p(D)\, dD} + \chi_0 B \tag{4}$$

where D is a dimensionality variable, L is the Langevin function and p can be any probability distribution function. The last term from Eq. (4) represents the field independent magnetic susceptibility χ_0.

3. Experimental procedure

3.1. Sample preparation

For the catalyst samples preparation, the chemical reagents used were $Ni(NO)_3.6H_2O$ p.a., $Cr(NO_3)_3.9H_2O$ p.a., $Al(NO_3)_3.9H_2O$ p.a. and NaOH p.a. To obtain Ni/Cr_2O_3 catalyst sample, the co-precipitation was carried out at room temperature by addition of a solution containing a mixture of nickel and chromium nitrates (ca. 0.5 molar) to a sodium hydroxide solution (ca. 1 molar) with vigorous stirring. The ratio between nitrates was chosen in such a way to obtain the desired atomic percentage of nickel, defined by X = [at. Ni/(at. Ni+Cr)] x 100%. Both Ni(II) and Cr(III) quantitatively precipitated during the preparation conditions allowing in this way to obtain the catalyst samples with initially determined Ni/Cr atomic ratios. The Ni/Al_2O_3 catalyst sample was prepared in the same way by co-precipitation of a solution containing a mixture of nickel and aluminium nitrates. The freshly precipitated sample was filtered and washed with double distilled water. The sodium and nitrate ions were thoroughly removed by repeating (6-8 times) the cycle of stirring with double distilled water, followed by filtering. The sample was dried at 378 K, calcined in a stream of nitrogen at 613 K, and reduced in flowing hydrogen at 623 K. The resulted sample is pyrophoric and ignites spontaneously in air atmosphere. In order to be handled in air the catalyst sample was passivated at room temperature in flowing nitrogen with low oxygen concentration (ca. 0.2%). The catalyst samples were reactivated prior to use by reduction in situ, in hydrogen flow, at 623 K. The nickel black sample was prepared by precipitation of a solution of nickel nitrate with a sodium hydroxide solution. The procedure continued as described above.

3.2. Measurement methods

The X-ray diffraction data of the black Ni powder and supported nickel catalysts were collected at room temperature using a vertical powder diffractometer in Bragg-Brentano geometry installed on Bruker D8 ADVANCE setup at λ =1.54184 Å. The typical experimental conditions were: 5 seconds for each step, initial angle $2\theta=40^0$, step 0.02^0 and the whole spectra were measured on 3251 points. The magnetic studies of the investigated samples have been both performed by the extraction method, in a continuous magnetic field of up to 10 T, and in a vibrating sample magnetometer using a maximum applied field of 10 T. The magnetization measurements in zero-field cooled (ZFC) and field-cooled (FC) of the 85 at. % Ni/Al_2O_3 and 85 at. % Ni/Cr_2O_3 samples were measured in temperature range 4-300 K. For ZFC measurements, the samples are first cooled from room temperature to 4 K without any external applied magnetic field. Then, a magnetic field of 0.05 T is applied and magnetization is recorded during the warming of the samples up to 300 K. The FC curves, for both samples, were obtained by cooling the samples from room temperature to 4 K in a magnetic field of 0.05 T, followed by the magnetization measurement, in the same magnetic field, during the warming of the samples from 4 to 300 K.

4. Results and discussion

4.1. XRD results

In order to obtain accurate values of the crystallite size and microstrain parameter we have to take good care of experimental measurements and XRD data analysis. There are three main systematic errors that could appear in the data analysis: uncorrected constant background, truncation and the effect of the sampling for the observed profile at a finite number of points that appear in discrete Fourier analysis [10]. These all are influencing the Fourier analysis validity. A global approximation of the XRLP is adopted instead of the discrete calculus in order to minimize

the propagation of these systematic errors. Therefore, the diffraction line broadening was analytically calculated using the GFF and the Voigt distribution facilities. The robustness of the GFF and Voigt approximation for the XRLP arise from the possibility of using the analytical form of the Fourier transform instead of a numerical fast Fourier transform (FFT). In this way, the validity of the microstructural parameters are closely related to accuracy of the Fourier transform magnitude of the true XRLP.

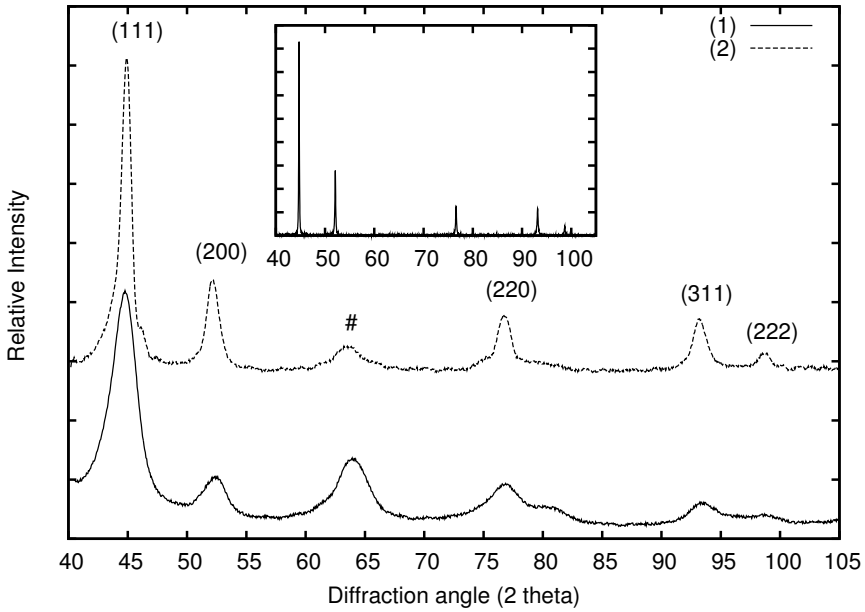

Fig. 1 The relative intensity of experimental XRLP: (1) – 85at. % Ni/Al_2O_3, (2) – 85at. % Ni/Cr_2O_3. # - contribution of metal oxide support. Inset: the spectrum of the reference black Ni powder.

We processed (111), (200), (220), (311) and (222) XRLP for black Ni powder as well as for 85 at. % Ni/Al_2O_3 and 85 at. %Ni/Cr_2O_3. Their experimental relative intensities with respect to the2θ values are shown in Fig. 1. The silicon powder was used for correction of the instrumental broadening effect. The next steps consist in the background correction of XRLP by polynomial procedures and the determination of the best parameters of GFF and Voigt distributions by nonlinear least squares fit. In order to determine the nanostructural parameters contained in Eq. (1), we computed the Fourier transforms of the true XRLP. The global structural parameters obtained for the investigated samples, extracted from our analysis, are summarized in Table 1.

Table 1 Global structural parameters for the investigated samples.

Sample	**Scherrer method**		**Warren-Averbach analysis**						
	GFF	**Voigt**	**Single order**					**Double Voigt order (111) - (222)**	
	D_{Sch} [nm]	**D_{Sch} [nm]**	**GFF**			**Voigt**		**D_{dV} [nm]**	**$\langle\varepsilon^2\rangle^{1/2}\times10^3$**
			D_s [nm]	**$\langle\varepsilon^2\rangle^{1/2}\times10^3$**	**GoF (%)**	**D_s [nm]**	**GoF (%)**		
Reference black Ni									
(111)	74.1	64.1	54.2	0.718	3.74	55.7	6.61	55.8	0.666
(200)	60.6	69.3	44.1	0.920	3.99	53.9	1.97		
(220)	58.5	76.7	44.1	0.921	2.63	49.2	1.18		

Sample	Scherrer method		Warren-Averbach analysis						
	GFF	Voigt	Single order					Double Voigt order (111) - (222)	
	D_{Sch} [nm]	D_{Sch} [nm]	GFF			Voigt		D_{dV} [nm]	$\langle\varepsilon^2\rangle^{1/2}\times10^3$
			D_s [nm]	$\langle\varepsilon^2\rangle^{1/2}\times10^3$	GoF (%)	D_s [nm]	GoF (%)		
(311)	56.8	48.8	44.6	0.915	3.84	44.3	1.21		
(222)	60.6	76.3	45.6	0.923	3.24	51.9	2.17		
average	**62.1**	**67**	**46.5**			**51**			
85 at.% Ni/Al_2O_3									
(111)	4.3	3.9	4.1	8.842	5.35	5.7	6.19	3.1	9.04
(200)	5.6	3.6	5.6	8.593	5.18	5.8	4.73		
(220)	5.4	4.2	2.1	9.320	8.63	4.7	5.02		
(311)	5.2	4.9	3.6	9.015	7.45	3.5	7.04		
(222)	7.0	7.3	6.5	8.808	4.64	6.1	3.84		
average	**5.5**	**4.8**	**4.4**			**4.6**			
85 at. % Ni/Cr_2O_3									
(111)	8.7	8.7	8.8	2.518	7.77	6.8	8.32	6.3	2.75
(200)	8.4	8.3	8.2	2.511	8.88	9.7	9.18		
(220)	7.2	8.6	7.4	2.638	7.71	5.5	8.91		
(311)	9.3	8.8	9.4	2.321	7.92	8.5	8.52		
(222)	8.7	11.1	8.8	2.524	6.11	9.1	7.94		
average	**8.5**	**9.1**	**8.5**			**7.9**			

The crystallites size obtained from the Scherrer method are contained in the second and the third columns. The forth up to the eighth columns contain the average crystallite size, the microstrain parameter and the goodness of the fit by single X-ray profile Fourier analysis approximated by GFF and Voigt distributions [2, 7]. The last two columns provide the same parameters as the ones determined by double Voigt method [3]. The D_{dV} are the average crystallite size determined from the crystallite distribution functions illustrated in Fig. 2.

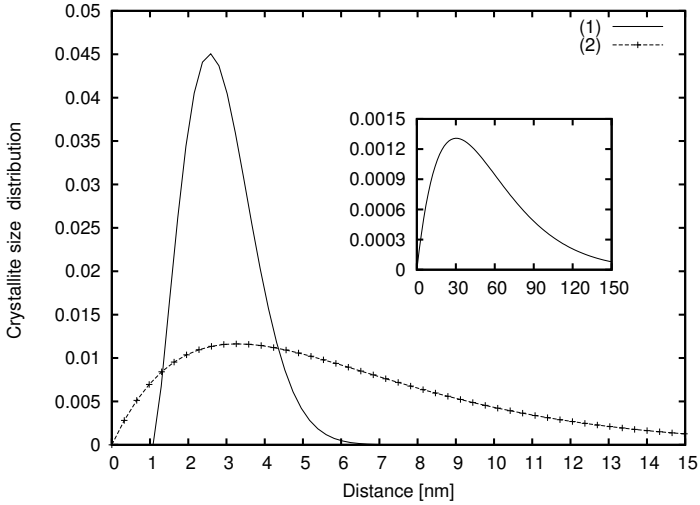

Fig. 2 The crystallite size distribution functions determined by double Voigt method: (1) – 85at. % Ni/Al_2O_3, (2) – 85at. % Ni/Cr_2O_3. Inset: the crystallite size distribution of the reference black Ni powder

The microstrain parameter of the lattice, $<\varepsilon_{hkl}^2>^{1/2}$, can also be correlated with the effective crystallite size in the following way: the value of the effective crystallite size increases when the microstrain value decreases. Because the Scherrer equation does not take into account the lattice strains sometimes having the size of the nanocrystallites, D_{Sch} determined by it are greater than results obtained by Eq. (1). Therefore, the values from the second and the third columns of Table 1 are less reliable than the results obtained via the Warren-Averbach method based on single X-ray profile Fourier analysis and double Voigt method. The crystallites size differences of D_s and D_{dV}, determined by second and third methods, are due to the different type of the analytical approximation techniques adopted [3, 11, 12]. The calculated uncertainties of the global parameters are between 5 and 8 percentages. The goodness of the fit, GoF, contained in the sixth and eighth columns of the Table 1, describe the degree of approximation of the XRLP. Moreover, they indicate the most reliable crystallite size values.

4.2. Magnetization results

The magnetization measurements in zero-field cooled (ZFC) and field-cooled (FC) of both supported Ni catalysts are shown in Fig. 3.

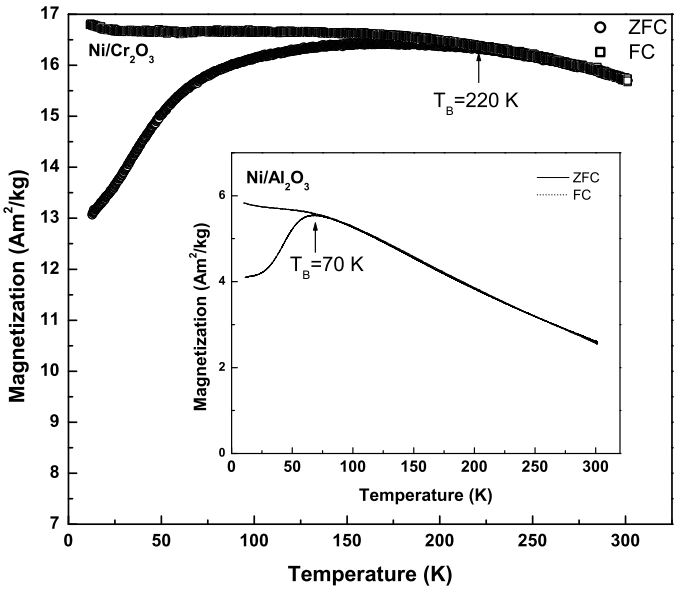

Fig. 3 The magnetization as a function of temperature obtained in ZFC and FC modes for 85at. % Ni/Cr_2O_3. Inset: 85at. % Ni/Al_2O_3.

For both 85 at. % Ni/Al_2O_3 and 85 at. % Ni/Cr_2O_3 samples, the FC and ZFC branches merge each other at 70 K and 220 K, respectively. These temperatures are related to the blocking temperature T_B of the superparamagnetic nanoparticles. However, similar magnetic analysis performed on the reference black Ni powder, not illustrated here, gives completely different M(T) curves. Due to large particle size of the black Ni powder we could not evaluate the blocking temperature up to room temperature, suggesting that it has a ferromagnetic behaviour. For particles with uniaxial anisotropy, the relation between critical volume V_c and blocking temperature T_B is given by the following relation [6],

$$V_c = \frac{25 k_B T_B}{K} \tag{5}$$

If we consider a spherical shape of the Ni nanoparticles and assuming for the anisotropy constant K a mean value of about $2x10^4$ J/m^3 [5], the Eq (5) gives us the critical diameters of the particle, under which the superparamagnetic behaviour is observed. The estimated values are 13.2 nm for Ni/Al_2O_3 and 19.1 for Ni/Cr_2O_3. The average diameters calculated from XRD measurements are around 5 *nm* and 8 *nm* for Ni/Al_2O_3 and Ni/Cr_2O_3, respectively. Because these values are much smaller than the critical ones determined from the magnetic analysis, we can admit that under the blocking temperature the particles have a superparamagnetic behaviour. Furthermore the slope of the M(B) curves at 300K, in the low magnetic field region (Figure 4), is smaller than one specific to a ferromagnetic material and much bigger than one specific to a paramagnetic material confirming once more that our samples present a superparamagnetic behaviour.

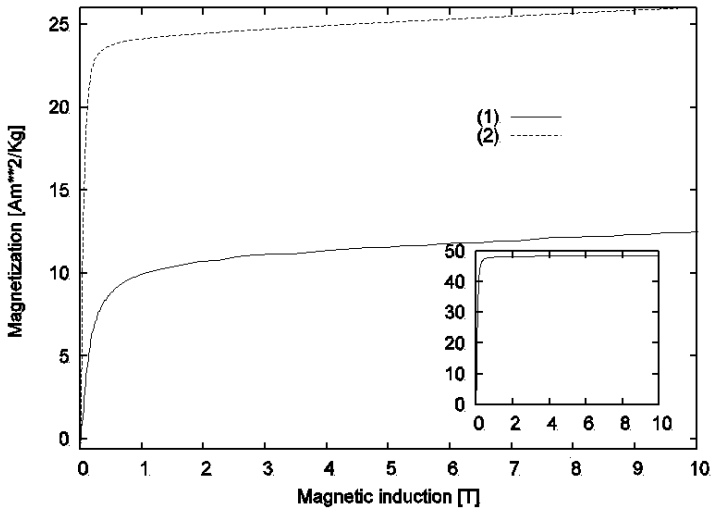

Fig. 4 The magnetization versus magnetic induction: (1) – 85at. % Ni/Al_2O_3, (2) – 85at. % Ni/Cr_2O_3. Inset: Field dependence of the magnetization for the reference black Ni powder.

We come back to the magnetisation evolution of 85 at. % Ni/Al_2O_3 and 85 at. % Ni/Cr_2O_3, at 300K, as a function of the magnetic induction presented in Fig.4. Appling the superparamagnetic theory, for our investigated samples, and using different probability density functions in according with Eq.(4), the mean particle diameter D_m, the standard deviation σ and the independent susceptibility χ_0 were evaluated. The numerical simulations have been realized by a computer code developed in language of the *gnuplot* software. The input data for test run are: average volume fractions, ε is 0.867 for *85 at. %Ni/Al_2O_3* and 0.814 for *85 at. %Ni/Cr_2O_3* determined from the atomic concentrations of investigated samples, the volume spontaneous magnetization value, M_s=57.3 Am^2/Kg [13], the density, ρ_{Ni}=8900 Kg/m^3, Boltzmann constant, k_B=0.13806505×10^{-22} J/K and experimental curve magnetizations presented in Fig. 4. Consequently, we considered a spherical form of the particles and the following probability density functions: normal, chisqure, erlang, gamma, gumbel, logistic, lognormal, maxwell and poisson [9]. Then we have calculated the mean diameters, D_m and the standard deviations, σ. Their values are presented in Table 2.

Table 2 The mean diameters and the standard deviations obtained from numerical simulations of the magnetization curves

Sample	**Normal**		**Chisquare**		**Erlang**		**Gamma**		**Gumbel**		**Logistic**		**Lognormal**		**Maxwell**		**Poisson**	
	D_m [nm]	**σ**	**D_m** [nm]	**σ**	**D_m** [nm]	**σ**	**D_m** [nm]	**σ**	**D_m** [nm]	**σ**	**D_m** [nm]	**σ**	**D_m** [nm]	**σ**	**D_m** [nm]	**σ**	**D_m** [nm]	**σ**
85 at. % Ni/Al_2O_3	3.99	1.69	5.30	0.86	4.87	1.25	5.19	1.07	4.92	1.19	4.60	1.39	5.06	1.28	5.05	2.40	3.28	1.81
85 at. % Ni/Cr_2O_3	9.88	0.37	9.52	1.45	9.70	1.57	12.52	1.96	9.89	0.53	10.78	0.76	10.05	1.12	8.60	4.09	9.46	3.07

The uncertainties of the probability distribution functions parameters are less than six percentages and the goodness of the fit of the magnetization curves are smaller than 5 percentages. The values of χ_0 are 0.162161±0.0034 Am^2/KgT and 0.1108±0.013 Am^2/KgT for Ni/Al_2O_3 and Ni/Cr_2O_3, respectively. Figs. 5 and 6 illustrate experimental magnetization curves together with the calculated ones for the best approximation distribution functions.

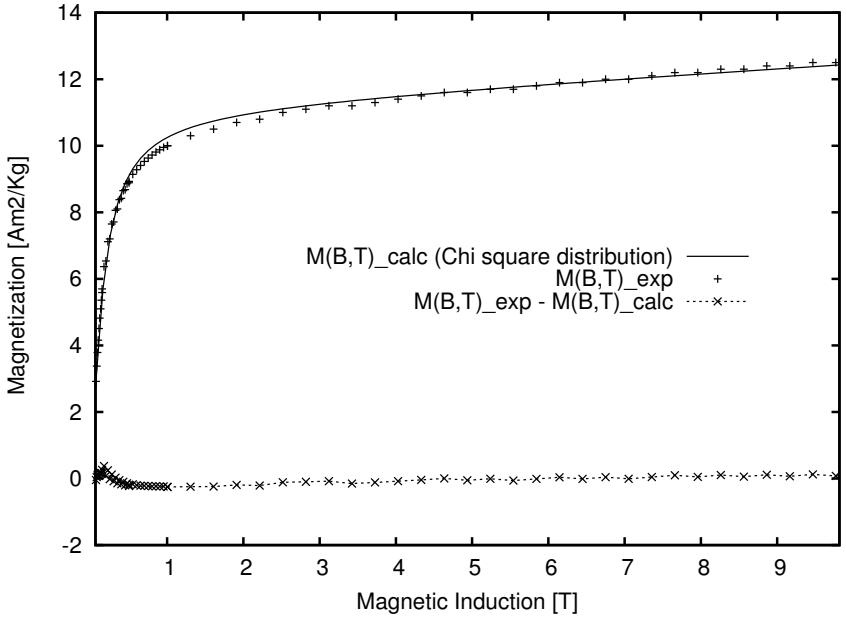

Fig. 5 The experimental and calculated magnetization approximated by chisquare probability distribution function for 85at. % Ni/Al_2O_3 sample.

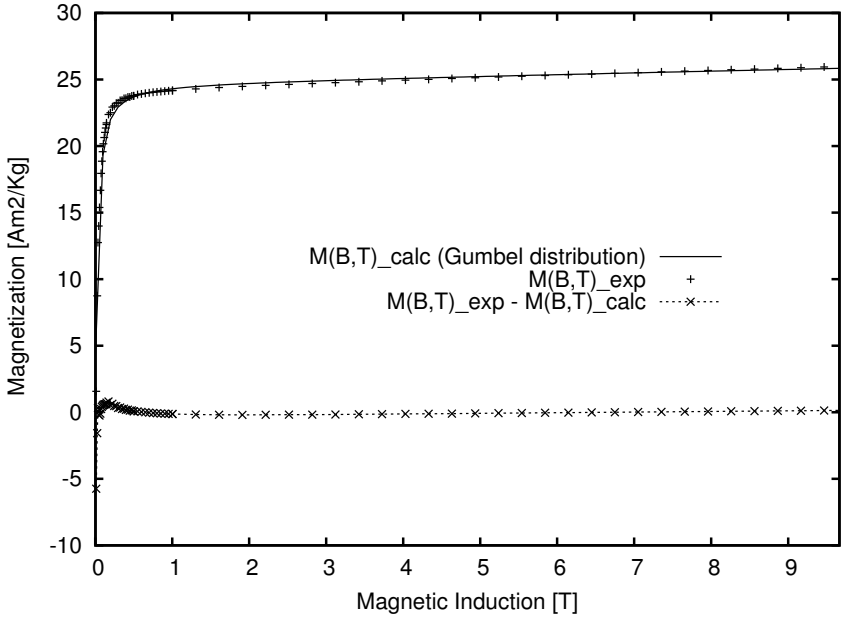

Fig. 6 The experimental and calculated magnetization approximated by gumbel probability distribution function for 85at. % Ni/Cr_2O_3 sample.

The crystallites size determined from XRD analysis using Warren-Averbach method are smaller than those obtained via magnetization measurements. This suggests that the magnetic grains are formed from an ensemble of crystallites coupled through exchange interactions. Additional measurements are needed in order to prove the interparticles interactions. These interactions between the superparamagnetic nanopaticles are often present and there are several

models that consider them [14]. If we take into account the crystallite size associated to different reflexion planes obtained by X-ray diffraction method; the spherical form adopted here is not the best approximation for nanoparticles shape. The subsequent elaboration of a geometrical model of the crystallite volumes based on X-ray diffraction measurements and introducing the resulted model by *V(D)* function in Eq.(4) will lead to more accurate results.

The particle diameters of Ni supported on alumina are smaller than those supported on chromia. Similar results were obtained previously in the literature [15]. They shown that in the case of supported Ni catalysts prepared by coprecipitation method, the alumina is a better dispersant than chromia.

Hydrogen chemisorptions, transmission electron microscopy, electronic paramagnetic resonance and other methods could also be used to determine grain size of particles by taking into account a prior geometrical form for the grains. There is a large difference between the grain size and crystallite size due to the physical meaning of the two concepts. It is possible that the grains of the active metal are built up of many nickel crystallites.

5. Conclusion

In the present paper we have shown that, in addition to XRD experiments with their specific advantages, magnetization measurements can add more information for understanding bulk nanostructure of the nickel nanoparticles supported on aluminium oxide and chromium oxide. The conclusions that can be drawn from these studies are:

(i) For XRLP analysis, the global approximation are applied rather that numerical Fourier analysis. The former analysis is better than a numerical calculation because it can minimise the systematic errors that appear in the traditional analysis. Each of the three techniques gave the average particle size with small differences due to analytical approximated methods used in Warren-Averbach analysis. Because Scherrer method does not take into account the lattice strains the crystallite size are less reliable in comparison with Fourier techniques;

(ii) The investigated samples present a superparamagnetic behaviour, crystallites size distribution and their standard deviations were determined;

(iii) The dimensionality results obtained from XRD and magnetic measurements are in good correlation but the spherical volume approximation of the crystallites must be improved;

(iv) The larger values of the diameters obtained via magnetic measurements suggest the presence of the exchange interactions between the nanoparticles;

(v) The best approximation of the magnetization curve was obtained using chisquare and gumbel distribution functions;

(vi) The reported structural results represent an important key in the explanation of the catalytic activity which is strongly correlated with the dimension of the Ni nanoparticles.

References

[1] B.E. Warren, X-Ray Diffraction, Addison-Wesley Publishing Company, pp. 264-291 (1969).
[2] N. Aldea, E. Indrea, Comput Phys Commun **60**, 155-163 (1990).
[3] D. Balzar, Voigt Function Model in Diffraction Line Broadening Analysis, in: R.L. Snyder, H.J. Bunge, J. Fiala (Eds), Defect and Microstructure Analysis by Diffraction, International Union of Crystallography Monographs on Crystallography No 10, Oxford University Press, New York, pp. 94-126 (1999) .
[4] N. Aldea, B. Barz, T.D. Silipas, F. Aldea, Zhonghua Wu, J Optoelectron Adv Mater **7**(6), 3093-3100 (2005).
[5] C. Estournes, T. Lutz, J. Happich, T. Quaranta, P. Wissler, J.L. Guille, J Magn Magn Mater **173**, 83-92 (1997).
[6] S.K. Sharma, R. Kumar, V.V.S. Kumar, S.N. Dolia, Indian J Pure Appl Phys **45**, 16-20 (2007).
[7] N. Aldea, R. Turcu, A. Nan, I. Craciunescu, O. Pana, Y. Xie, Zhonghua Wu, D. Bica, L. Vekas, F. Matei, J Nanopart Res **11**(6), 1429-1439 (2009).

[8] N. Aldea, C. Tiusan, R. Zapotinschi, A new approach used to evaluation the crystallite size of supported metal calalysts by single X-ray profile Fourier transform implemented on maple V, in: P. Borcherds, M. Bubak, A. Maksymowicz (Eds), Proceedings of the 8th joint EPS-APS International Conference on Physics Computing, Krakow, pp. 391-394 (1996).
[9] M. Abramowich, A. Stegun, Handbook of mathematical functions, Dover, New York, pp. 297-309 and pp. 929-930 (1968).
[10] R.A. Young, R.J. Gerdes, A.J.C. Wilson, Acta Cryst. **22**, 155-162 (1967).
[11] F. Raiteri, A. Senin, G. Fagherazzi, J Mat Sci **13**, 1717-1724 (1978).
[12] N. Aldea, R. Zapotinschi, C. Cosma, Fresenius J Anal Chem **355**, 367-369 (1995).
[13] J. William, D. Callister, Materials Science and Engineering. An introduction, 6 th edn. John Wiley & Sons, Inc, pp 681-681 (2003).
[14] M. Knobel, W.C. Nunes, L.M. Socolovsky, E. De Biasi, J.M. Vargas and J.C. Denardin, J. Nanosci. Nanotechnol. **8** (6), 2836-2857 (2008).
[15] P. Marginean, Al. Olariu, J. Catal **95**, 1-12 (1985).